Contents lists available at ScienceDirect

Innovative Food Science and Emerging Technologies

journal homepage: www.elsevier.com

Improvement of radio frequency (RF) heating uniformity for peanuts with a new strategy using computational modeling

Shuang Zhang [a], Zhi Huang [a], Shaojin Wang [a, b, *]

[a] Northwest A&F University, College of Mechanical and Electronic Engineering, Yangling, Shaanxi 712100, China
[b] Department of Biological Systems Engineering, Washington State University, 213 L.J. Smith Hall, Pullman, WA 99164-6120, USA

ARTICLE INFO

Article history:
Received 4 December 2016
Received in revised form 12 February 2017
Accepted 19 February 2017
Available online xxx

Keywords:
Computer simulation
Radio frequency
Heating uniformity
Mica container
Peanut

ABSTRACT

Radio frequency (RF) heating has been considered as an alternative method to traditional thermal treatments for postharvest pasteurization and disinfestations. However, the non-uniform heating in food samples is the main obstacle to be urgently solved. In this study, mica plates were placed on top of the samples with polypropylene blocks placed in between the samples as a new strategy to improve the RF heating uniformity. A computer simulation model was developed based on the commercial software COMSOL to evaluate the temperature distributions. Experiments with peanut samples placed in three dimensions of containers were conducted to validate the simulation model. The results showed that adding mica plates with the similar dimension to the cold spot of samples and increasing the plate thickness effectively improved the RF heating uniformity. Adding polypropylene blocks raised sample average temperatures and finally optimized the RF heating uniformity.

1. Introduction

Fungal infection and insect infestation are the major problems for peanuts storage, which cause huge quantitative and qualitative damages. The insects destroy the peanut quality through feeding and webbing, contaminating with fecal matter, and introducing diseases. Mold like *Aspergillus flavus* degrades the peanut quality by contamination with the aflatoxins, which are harmful to human and animal health (Hill, Blankenship, Cole, & Sanders, 1983). Many methods have been used for disinfesting and pasteurizing postharvest agricultural products, such as conventional thermal treatment, chemical fumigation, irradiation, controlled atmospheres and cold storage (Follett et al., 2013; Hertwig, Kai, Ehlbeck, Knorr, & Schlüter, 2015; Jiao et al., 2013; Kanapitsas, Batrinou, Aravantinos, & Markaki, 2015; Suhem, Matan, Nisoa, & Matan, 2013). Since each of these has limitations in terms of low efficiency, high cost and negative effects on environment or product quality, novel heating technologies need to be developed to explore their effectiveness on insect and mold control for peanuts.

Radio frequency (RF) energy has long been studied as an application for postharvest insect control in agricultural commodities for its high efficiency and non-damage to environment (Wang et al., 2001; Wang, Tang, Johnson, & Cavalieri, 2013; Zhou & Wang, 2016). RF technology has also been studied for pasteurization in many food materials, such as almond (Gao, Tang, Villa-Rojas, Wang, & Wang, 2011), corn (Zheng, Zhang, Zhou & Wang, 2016), and pepper (Jeong & Kang, 2014). However, non-uniformity is still the major problem for RF heating, especially for samples with intermediate and high moisture contents (Farag, Marra, Lyng, Morgan, & Cronin, 2010; Fu, 2008; Hou, Huang, Kou, & Wang, 2016). The uneven electric field distribution caused by different dielectric properties between samples and surrounding media always results in overheating in corners and edges of rectangular containers (Birla, Wang, Tang, & Hallman, 2004). Several methods have been studied to improve the RF heating uniformity like reducing edge and corner temperatures, combination with hot air heating (Zhou, Ling, Zheng, Zhang, & Wang, 2015), intermittent mixing (Chen, Wang, Li, & Wang, 2015; Wang, Yue, Tang, & Chen, 2005), sample movement (Chen, Huang, Wang, Li, & Wang, 2016), and changing the container material (Huang, Zhang, Marra, & Wang, 2016; Zheng, Zhang, Zhou, & Wang, 2016). However, it is inconvenient and time consuming to explore new methods to improve heating uniformity by changing parameters with experiments. Computer simulation may serve as an effective tool for rapid analysis of RF heating mechanism in food samples without conducting experiments.

The finite element modeling method has been used to improve heating uniformity by changing various factors that affect the temperature distribution in food samples. Tiwari, Wang, Tang, and Birla (2011a) studied the influence of sample dimension, shape, relative position between the RF electrodes, and dielectric properties of the sample and surrounding medium on RF power distribution in foods, and found that the sample dimension greatly affects RF power density and heating uniformity. Huang, Marra and Wang (2016) developed a simulation model based on COMSOL software to investigate the relationship of dielectric properties and density of surrounding container

* Corresponding author at: Northwest A&F University, College of Mechanical and Electronic Engineering, Yangling, Shaanxi 712100, China.
Email address: shaojinwang@nwsuaf.edu.cn (S. Wang)

http://dx.doi.org/10.1016/j.ifset.2017.02.009
1466-8564/

with treated products on RF heating uniformity, and established correlations when the best heating uniformity was obtained. The results showed that the uniformity index was the lowest when the dielectric constant of the container and sample were comparable, with the loss factor of the container within 0.01–0.1% of the sample's one. Jiao, Tang, and Wang (2014) improved the heating uniformity of peanut butter by surrounding the sample with polyetherimide, which has similar dielectric properties to those of peanut butter. There has no research applying these methods on improving peanuts heating uniformity. It is desirable to introduce a new container material (mica) with similar dielectric constant to peanut kernels and low loss factor values (Zhang, Zhou, Ling, & Wang, 2016) to improve RF heating uniformity.

The objectives of this study were to: (1) measure the thermal properties of peanut kernels at different temperatures, (2) establish a computer simulation model to predict temperature distribution in three different layers (top, middle and bottom) with peanut kernels placed in three different dimensions of mica containers, (3) validate the simulation model with a 6 kW, 27.12 MHz RF system, and (4) apply the validated simulation model to evaluate the heating uniformity of peanut kernels as affected by the dimension of mica plates and polypropylene blocks.

2. Materials and methods

2.1. Sample preparation

Peanut kernels with initial moisture content of 10.70% w.b. were purchased from a local supermarket in Yangling, Shaanxi, China. All the peanut samples were stored in polyethylene bags in a refrigerator (BD/BC-297KMQ, Midea Refrigeration Division, Hefei, China) at 3 ± 1 °C before test. Prior to RF treatments, all samples were taken out of the refrigerator and put into an incubator (BSC-150, Boxun Industry & Commerce Co., Ltd., Shanghai, China) for > 12 h to equilibrate their temperature to 25 ± 0.5 °C.

2.2. Physical properties of food material

Thermal properties (specific heat (c_p, J kg^{-1} °C^{-1}) and thermal conductivity (k, W m^{-1} °C^{-1})) of peanuts were measured with a thermal property analyzer (KD2 Pro, Decagon Inc., Pullman, WA, USA) and a SH-1 sensor. The samples were put in a glass beaker (in diameter of 31.75 mm and height of 47.15 mm) fixed with a steel holder. The two parallel needles of SH-1 sensor were inserted into samples with depth of 15 mm. The glass beaker was immersed in the water bath to allow the peanut samples to reach the selected temperatures (25 to 85 °C with an interval of 10 °C). A Type-T thermocouple thermometer (TMQSS-020-6, Omega Engineering Ltd., CT, USA) was inserted into the center of samples for guaranteeing the sample to reach the appointed temperatures. Dielectric properties of peanut kernels at moisture content of 10–30%, temperature range of 25–85 °C, and frequency range of 10 MHz to 4.5 GHz were measured and reported before (Zhang, Zhou, Ling, & Wang, 2016). In this study, dielectric constant (ε') and loss factor (ε'') of peanut kernels at moisture content of 10.70%, frequency at 27 MHz, and temperature (T) range of 25–85 °C were calculated by the following equations (Zhang et al., 2016):

$$\varepsilon' = 1.92\times10^{-5}T^3 - 2.154\times10^{-3}T^2 + 0.0639T + 5.786 \quad (1)$$

$$\varepsilon'' = 8.23\times10^{-3}T^2 - 0.914T + 22.576 \quad (2)$$

2.3. Surrounding material and dimension selection

It has been reported in previous studies that the RF heating uniformity can be improved when the surrounding material dielectric constant is in a comparable range of the samples (Huang, Zhang, Marra and Wang, 2016; Tiwari et al., 2011a). Mica was chosen as the container material because its dielectric constant is similar to that of peanut kernels but with low loss factor (Table 1). To study the influence of the container dimension on RF heating uniformity, three different containers were used in both experiment and computer simulation. The small (300 × 200 × 60 mm^3) and medium (400 × 300 × 60 mm^3) containers were chosen for laboratory scale tests. The large (500 × 400 × 60 mm^3) container with the same width as the top electrode was chosen for industrial scale applications. Another method was studied to further improve RF heating uniformity. A polypropylene block was chosen to modify the distribution of electric field for its cheap, stable and high heat resistance.

2.4. Development of computer model

2.4.1. Physical model

A free-running oscillator, 6 kW, 27.12 MHz parallel plate RF heating system (COMBI 6-S, Strayfield International Limited, Workingham, UK) was used to study the heating uniformity of peanuts. The RF system consisted of cavity, generator, and applicator with top and bottom electrodes (Fig. 1). The space between the two electrodes formed an electromagnetic field when the generator provided electromagnetic energy to the applicator. The RF output power can be changed by adjusting the gap between the moving top electrode and the fixed bottom electrode. Peanut samples in three different dimensions of mica containers (300 × 200 × 60, 400 × 300 × 60, and 500 × 400 × 60 mm^3) were placed at the center of the bottom electrode.

2.4.2. Governing equations

The electric field intensity in the electromagnetic field can be obtained by solving the Maxwell's equation. Since the RF wavelength (11 m) is often much larger than the electrode gap, the Maxwell's equation can be simplified to Laplace equations (Alfaifi et al., 2014; Choi & Konrad, 1991; Metaxas, 1996):

Table 1
Electric and thermo-physical properties of materials used in computer simulation.

Material properties	Mica[a]	Polypropylene[b]	Aluminum[a]	Air[a]
Density (kg m^{-3})	2900	900	2700	1.2
Thermal conductivity (W m^{-1} K^{-1})	0.5	0.26	160	0.025
Heat capacity (J kg^{-1} K^{-1})	880	1800	900	1200
Dielectric constant (ε')	6	2.0	1	1
Loss factor (ε'')	0.0003	0.0023	0	0

[a] COMSOL material labrary (2012).

[b] Von Hippel (1954).

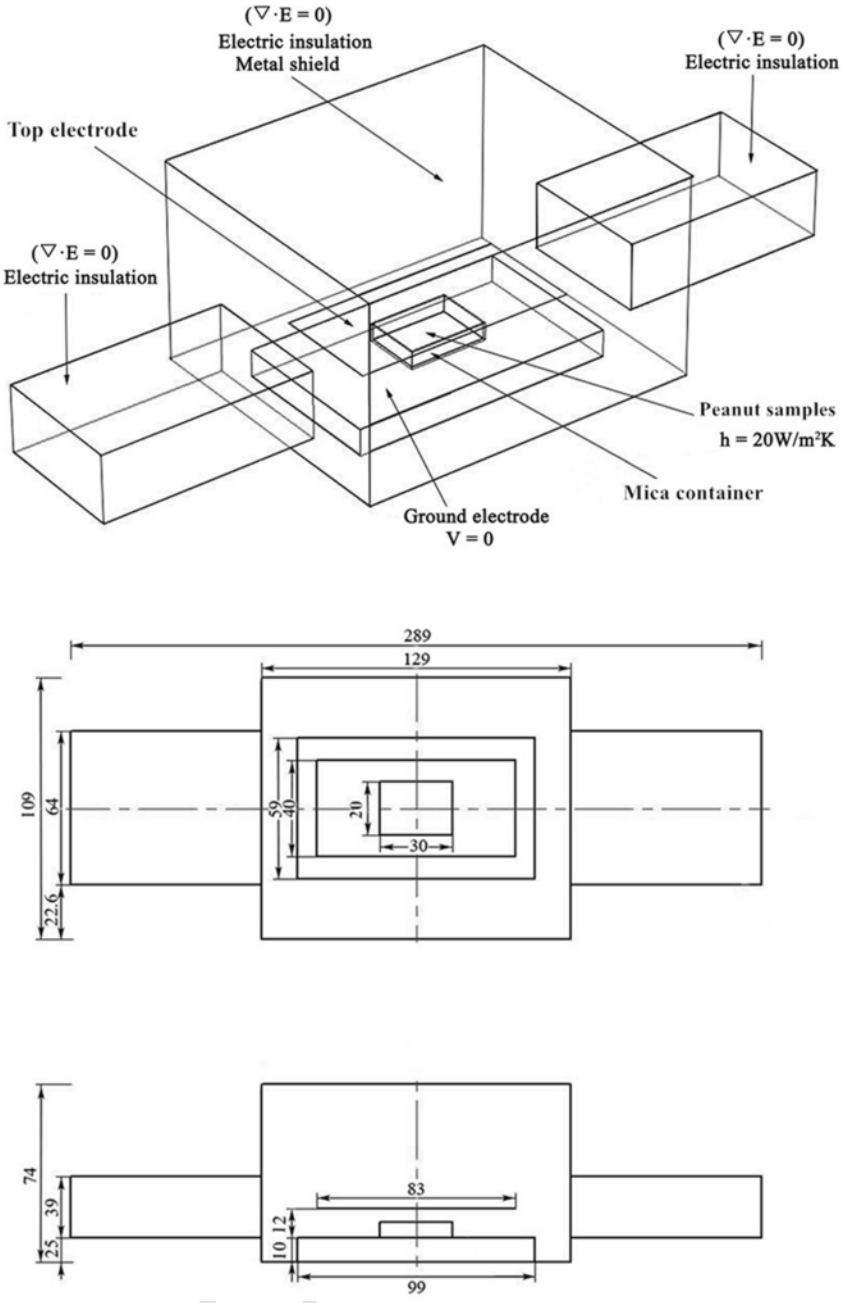

Fig. 1. 3-D Scheme (a) and dimensions of the 6 kW, 27.12 MHz RF system and food load (peanut kernels) used in simulation (all dimensions are in cm) (adapted from Huang, Zhu and Wang, 2015).

$$-\nabla \cdot \left(\left(\sigma + j2\pi f\varepsilon_0\varepsilon'\right)\nabla V\right) = 0 \tag{3}$$

where σ is the electrical conductivity of the heated material (S m^{-1}), $j = \sqrt{-1}$, f is the frequency (Hz), ε_0 is the permittivity of free space (8.86×10^{-12} F m^{-1}), and V is the voltage between the two electrodes (V).

When a dielectric material is placed between the two electrodes, the power conversion from electromagnetic energy to thermal energy is related to the working frequency, dielectric properties of treated material and the electric field density. The absorbed RF power in the material can be defined as (Huang, Zhu, Yan, & Wang, 2015; Ryynänen, 1995; Tiwari et al., 2011a; Tiwari, Wang, Tang, & Birla, 2011b):

$$Q = 2\pi f\varepsilon_0\varepsilon''|E|^2 \tag{4}$$

where Q is the power conversion to thermal energy in food materials (W m^{-3}), and $|E|$ is the electric field intensity in food materials (V m^{-1}).

The heat transfer inside the food sample is described as:

$$\rho C_P \frac{\partial T}{\partial t} = \vec{\nabla} \cdot k\vec{\nabla}T + Q \tag{5}$$

where $\partial T / \partial t$ is the heating rate of food materials (°C s^{-1}), ρ is the food density (kg m^{-3}), C_p and k are respectively their specific heat (J kg^{-1} K^{-1}) and thermal conductivity (W m^{-1} K^{-1}). Due to small temperature range, the thermal properties of mica, polypropylene, aluminum and air except for peanuts were taken as constant values shown in Table 1.

2.4.3. Initial and boundary conditions

The initial temperature of all simulation cases, including the air, mica container, peanut samples and two electrodes was set at 25 °C. The convection heat transfer boundary conditions were set at surfaces of peanuts exposed to the air with a heat transfer coefficient of $h = 20$ W m^{-2} K^{-1} (Huang, Zhu, Yan and Wang, 2015; Huang, Zhu, & Wang, 2015a). The top electrode was set as the electromagnetic source since it introduced high frequency electromagnetic energy from the generator to the heating cavity. The voltage on the top electrode was assumed to be constant during the RF heating since the electrode dimensions (0.83 × 0.4 m^2) were much lower than 30% of the RF wavelength (≈ 11 m). The top electrode voltage (V) can be estimated by the following equation (Zhu, Huang, & Wang, 2014):

$$V = 11242 \times I_a + 2029.9 \tag{6}$$

where I_a is the measured anode current (A).

On the basis of measured anode current of 0.45, 0.48 and 0.53 A for small, medium and large mica containers, respectively, the top electrode voltages were set at 7080, 7400 and 7900 V. All the metal shielding parts except for the top electrode were grounded and considered as electrically insulated $\nabla E = 0$ (Marra, Lyng, Romano, & Mckenna, 2007; Romano & Marra, 2008).

2.4.4. Simulation methodology

A finite element method (FEM) was used to solve the coupled electromagnetic and heat transfer equations (Joule heating model) with the commercial software, COMSOL (V4.3a, COMSOL Multiphysics, CnTech Co., LTD., Wuhan, China). The software was run on a Dell workstation with an Inter® Core™ i5-2400, 3.10-GHz processor and 8 GB RAM operating with a Windows 7 64-bit operating system. In this study, extremely fine tetrahedral meshes were generated in food samples and the top electrode, and normal dimension meshes were generated in all other parts. The result accuracy is mainly affected by the meshing size, and generally the small element size would result in more accurate results, but a considerable increase in computing time. The criteria of meshing were obtained when the predicted maximum temperature difference between successive calculations was < 0.1%. The main solution steps for the development of computer simulation model are shown in Fig. 2.

2.5. Model validation

To validate the computer simulation model, the 6 kW, 27.12 MHz pilot-scale RF system was used to heat peanut samples. About 2.35, 4.47, 7.25 kg peanuts were put into three different dimensions of mica containers (300 × 200 × 60, 400 × 300 × 60, and 500 × 400 × 60 mm^3) and placed at the center of the bottom electrode with an electrode gap of 130 mm. All the three containers were horizontally divided into three layers by two thin gauzes with mesh opening of 1 mm to easily map the surface temperature distribution (Fig. 3). The temperature at the geometric center of samples was recorded by a six-channel fiber optic temperature sensor system (HQ-FTS-D120, Heqi Technologies Inc., Xian, China) with an accuracy of ± 0.5 °C. In the experiment, thermal images of the sample top surface were taken after RF treatments. The lowest temperature location of the three surfaces was identified as the cold spot of the food sample.

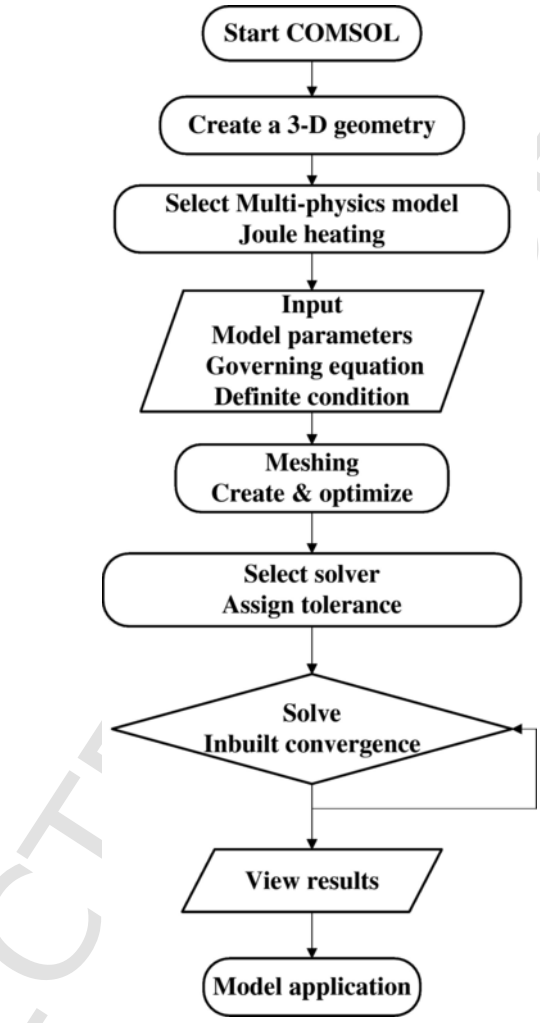

Fig. 2. Procedures and steps of building computer simulation model for RF heating by COMSOL software.

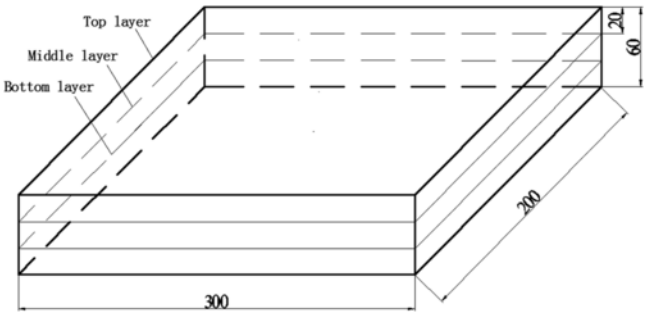

Fig. 3. Rectangular mica container split into three layers for surface temperature measurements.

In the computer simulation, the cold spot location was found from the volumetric temperature map with the model. In RF heating experiments, when the cold spot temperature of the food sample reached 70 °C that was selected based on inhibition of *Aspergillus flavus* in peanuts using RF energy (Jiao, Zhong, & Deng, 2016), the sample container was removed from the heating cavity. Therefore, the three container samples were subjected to RF heating for 420, 480 and 530 s, respectively. After the RF heating, the sample container was immediately moved out for surface temperature mapping. Before and immediately after the RF treatment was completed, the top layer surface temperature was measured by an infrared camera (DM63-S, DaLi Science and Technology Co., LTD, Zhejiang China) with an accuracy of ± 2 °C. Middle and bottom layers were mapped sequentially. The camera was calibrated by comparing the output temperature with the actual temperature measured with a calibrated thermocouple. All the thermal imaging measurements were completed within 30 s. Each experiment was replicated three times. The obtained temperature profiles of the sample center and temperature distribution of the three layers were further used to validate the computer simulation model.

2.6. Model application

2.6.1. Heating uniformity

After validation, the simulation model was used to evaluate how different container conformations and materials would affect the temperature uniformity of the RF treated samples. The heating uniformity of treated samples was evaluated by the uniformity index (UI), which has been used to evaluate the temperature distribution of samples in previous studies (Alfaifi et al., 2014):

$$\mathrm{UI} = \frac{\int_{V_{vol}} \left| T - T_{av} \right| dV_{vol}}{\left(T_{av} - T_{initial} \right) V_{vol}} \tag{7}$$

where T and T_{av} are the local and average temperatures (°C) in the food over the volume, $T_{initial}$ is the initial temperature of the food (°C), and V_{vol} is the volume of food (m^3).

2.6.2. Effect of mica plate dimension on heating uniformity

To study the effect of mica plate dimension on heating uniformity, simulations were performed with different lengths and widths of the three containers. The lengths of the mica plates were 100 to 250 mm, 100 to 350 mm and 100 to 400 mm for the small, medium and large mica containers, respectively. And the widths were 100 to 200 mm, 100 to 300 mm, and 100 to 400 mm, respectively (Fig. 4b). To explore the relationship between heating uniformity and mica plate dimension, the cold spot areas of three containers were obtained from both experimental and computer simulation methods. To further investigate the influence of the thickness of mica plates on heating uniformity, different thicknesses of mica plates were placed on peanut samples at the optimum length and width of each container.

2.6.3. Effect of polypropylene block dimension on heating uniformity

To improve the heating uniformity of peanut samples, a polypropylene block was placed at the center of the large container to change the distribution of the electric field. The widths, lengths, and depths of the polypropylene block ranged from 150 to 350 mm, 250 to 350 mm, and 20 to 40 mm (Fig. 4c), respectively.

3. Results and discussion

3.1. Temperature - dependent thermal properties of peanut kernels

The dielectric, thermal and physical properties of mica, polypropylene, aluminum and air were listed in Table 1, which are the essential parameters for computer modeling. Fig. 5 shows the temperature dependent thermal properties of peanuts at temperature range of 25 to 85 °C. The thermal conductivity increased from 0.233 to 0.294 W m^{-1} K^{-1}, and specific heat increased from 1883.3 to 2425.9 J kg^{-1} K^{-1} with the temperature increased from 25 to 85 °C. Similar trends were also found in other food materials, such as soybeans (Deshpande & Bal, 1999; Deshpande, Bal, & Ojha, 2007). These data were subjected to linear regression analysis and further used in computer simulation.

3.2. Computer model validation

Fig. 6 shows the surface contour plot of temperature distribution obtained from both experiment and simulation for the top, middle, and bottom layers of peanut samples placed in three different dimensions of mica containers. The surface temperature comparison of three layers demonstrated that the computer results matched well with the experimental ones. Based on both experimental and computer simulation results, the cold spot location was found to be at the center of each layer. The maximum temperature differences for the three containers in the middle layers were 5, 7 and 7 °C, respectively, which were located at the corners and edges. The result differences between simulations and experiments may be caused by the simplification of RF systems or ignored moisture and heat losses in the possible evaporation in samples. Table 2 compared the simulated and experimental average and standard deviation temperatures of peanut kernels in three horizontal layers for three containers. The experimental temperatures of three containers were slightly lower than the simulated ones, which may be caused by heat loss to the ambient air during the temperature measurement. The large standard deviation between the simulated results and experimental data may be caused by the high target temperature, which resulted in long heating time and large temperature differences between the hot and cold spots. Simulated and experimental temperature profiles measured at the geometry center of samples were also in good agreement (Fig. 7). Acceptable RMSE values of 0.014, 0.015 and 0.012 °C were observed for the small, medium and large containers, respectively. Both temperatures showed linear increase with the RF heating time. The sample temperatures in the smaller container increased faster than those in larger containers due to smaller heating volume under the similar RF heating power.

3.3. Effect of mica plate dimension on heating uniformity

The influence of the length and width of mica plates on heating uniformity for the small, medium, and large containers was listed in Tables 3, 4 and 5. When the length was fixed at 100 mm, the uniformity index (UI) was reduced from 0.146 to 0.142 with the width of mica plates increased from 100 to 300 mm, and then increased to 0.143 when the width increased to 400 mm for the large container (Table 5). Analogously, the UI value was reduced from 0.143 to 0.134 when the mica plate's length increased from 100 to 300 mm at width of 200 mm, and then UI increased to 0.136 when the plate length increased to 400 mm. The optimal heating uniformity was obtained when the length and width of the mica plate were at 300 and

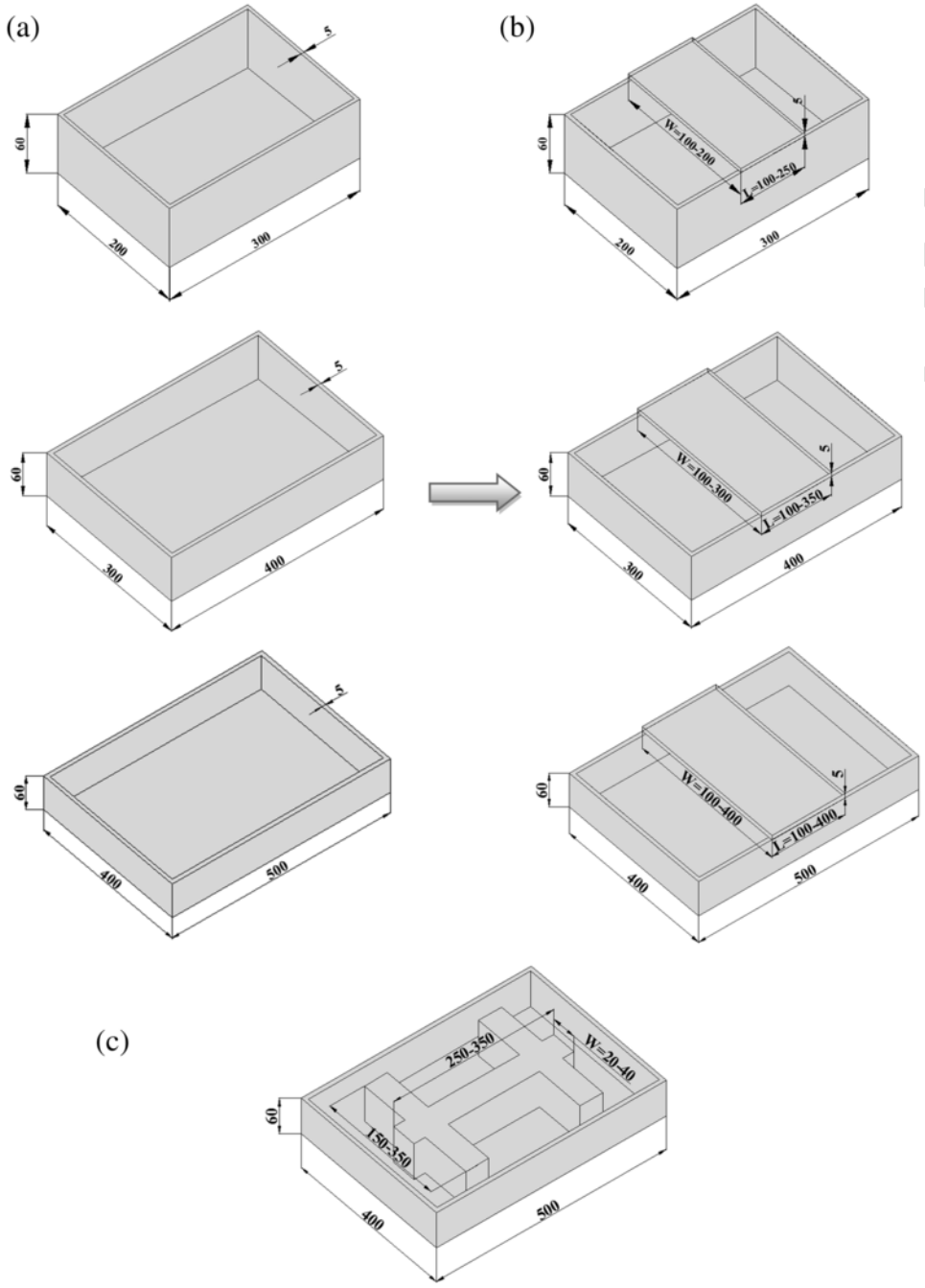

Fig. 4. Geometry of three different dimensions of mica containers without (a) and with (b) adding various dimensions of mica plates, or with various dimensions of polypropylene blocks in the large container (c) (all dimensions are in mm).

300 mm with the UI of 0.130. Similar phenomena were also observed in the small and medium containers. The lowest UI of the small and medium containers were 0.168 and 0.164, which were obtained when the length and width were at 200 and 150 mm, and 300 and 200 mm, respectively.

The electric field intensity of the three containers with and without mica plates was shown in Fig. 8. The electric field intensity at the center of containers increased when mica plates were added. The increase of heating uniformity with adding mica plates may be caused by the increased RF energy delivered to the cold spot of peanuts. More RF energy resulted in temperature increase in the cold spot of the sample and reduced the temperature differences between the overheating and the cold spot. Similar results can be found in peanut butter when polyetherimide blocks were added. (Jiao, Shi, Tang, Li, & Wang, 2015).

Fig. 9 shows the uniformity indexes varied with increasing mica plate thickness for the small, medium and large containers. All the uniformity indexes firstly decreased with increasing mica plate thickness, and then increased afterward. The plate thickness played an important role in improving RF heating uniformity of the peanuts temperature in small containers. The optimal UIs of 0.130, 0.120 and 0.126 were obtained with the mica plate thickness of 17, 15 and 9 mm

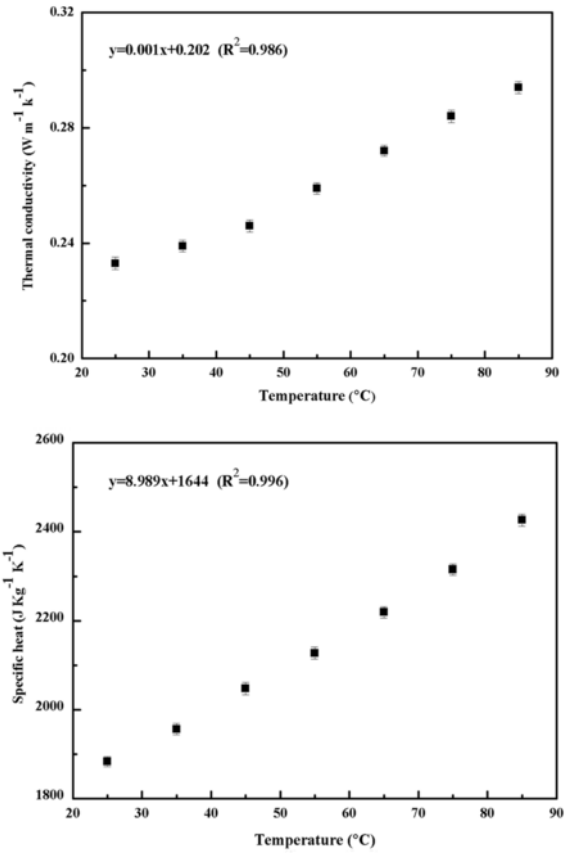

Fig. 5. Thermal conductivity (a) and specific heat (b) of peanut kernels with moisture contents of 10.70% w.b. at temperature range of 25 to 85 °C.

for small, medium and large containers, respectively. It has been reported that when a homogeneous food sample with a non-uniform thickness is placed between the electrodes, the thicker portion of the sample would normally absorb more energy and would heat up faster (Jiao, Shi, Tang, Li, & Wang, 2015; Mehdizadeh, 2009). Therefore, the increased thickness at the cold spot resulting from the addition of mica plates helped focus the electric field at the cold spot and raised the local temperature, resulting in better heating uniformity.

3.4. Influence of polypropylene block dimension on heating uniformity

The simulated volume average temperature and uniformity index of peanuts in the large container with various dimensions of polypropylene block were presented in Table 6. The temperature increased with increasing width, length and depth of polypropylene blocks. As the width and length of polypropylene blocks increased from 150 to 350 mm and from 250 to 350 mm, the average temperature increased from 77.57 to 79.13 °C at the depth of 20 mm. The uniformity index decreased from 0.140 to 0.136 when the width of the polypropylene blocks increased from 150 to 350 mm at the fixed length of 300 mm and depth of 30 mm. However, the uniformity index firstly decreased from 0.134 to 0.131 with the length increased from 250 to 300 mm, and then increased to 0.133 when the length increased to 350 mm. As the depth increased from 20 to 40 mm at the fixed width of 350 mm and length of 300 mm, the uniformity index decreased from 0.138 to 0.131. The optimal heating uniformity was obtained at the width of 350 mm, length of 300 mm, and depth of 40 mm for the large container. Therefore, in practical applications for a RF treatment, the heating uniformity can effectively be improved by placing polypropylene blocks among peanut samples.

4. Conclusions

A computer model was developed to explore the effectiveness of adding mica plates on the top of peanuts and polypropylene blocks among the peanuts to improve the heating uniformity of peanuts subjected to RF heating when the measured thermal properties of peanuts were used as a function of temperatures. Results from computer simulation and experimental methods showed good agreement for the temperature distribution of peanut samples in three different horizontal layers (top, middle, and bottom) placed in three different dimensions of mica containers. Corners and edges were heated more than center areas in all layers. Simulated results indicated that the use of adding mica plates on the cold spot and polypropylene blocks among peanuts had the potential to improve the heating uniformity of peanuts heated in RF systems. Furthermore, the model can be used to optimize the design parameters in the heating uniformity improvement methods. The optimal UI can be obtained at the mica plate thickness of 17, 15 and 9 mm for small, medium and large containers, respectively. The lowest uniformity index (0.120) was obtained with the mica plate (300 mm × 200 mm × 15 mm) for the medium container. Therefore, the exploration of new methods to improve uniformity in this study would be served as a first step in developing an effective RF pasteurization and disinfestations protocol for peanuts.

Acknowledgments

This research was conducted in the College of Mechanical and Electronic Engineering, Northwest A&F University, and supported by research grants from General Program of National Natural Science Foundation of China (31371853). The authors thank Long Chen, Hongxue Zhou, Ajuan Zheng, Rui Li and Kun Wang for their help in conducting experiments.

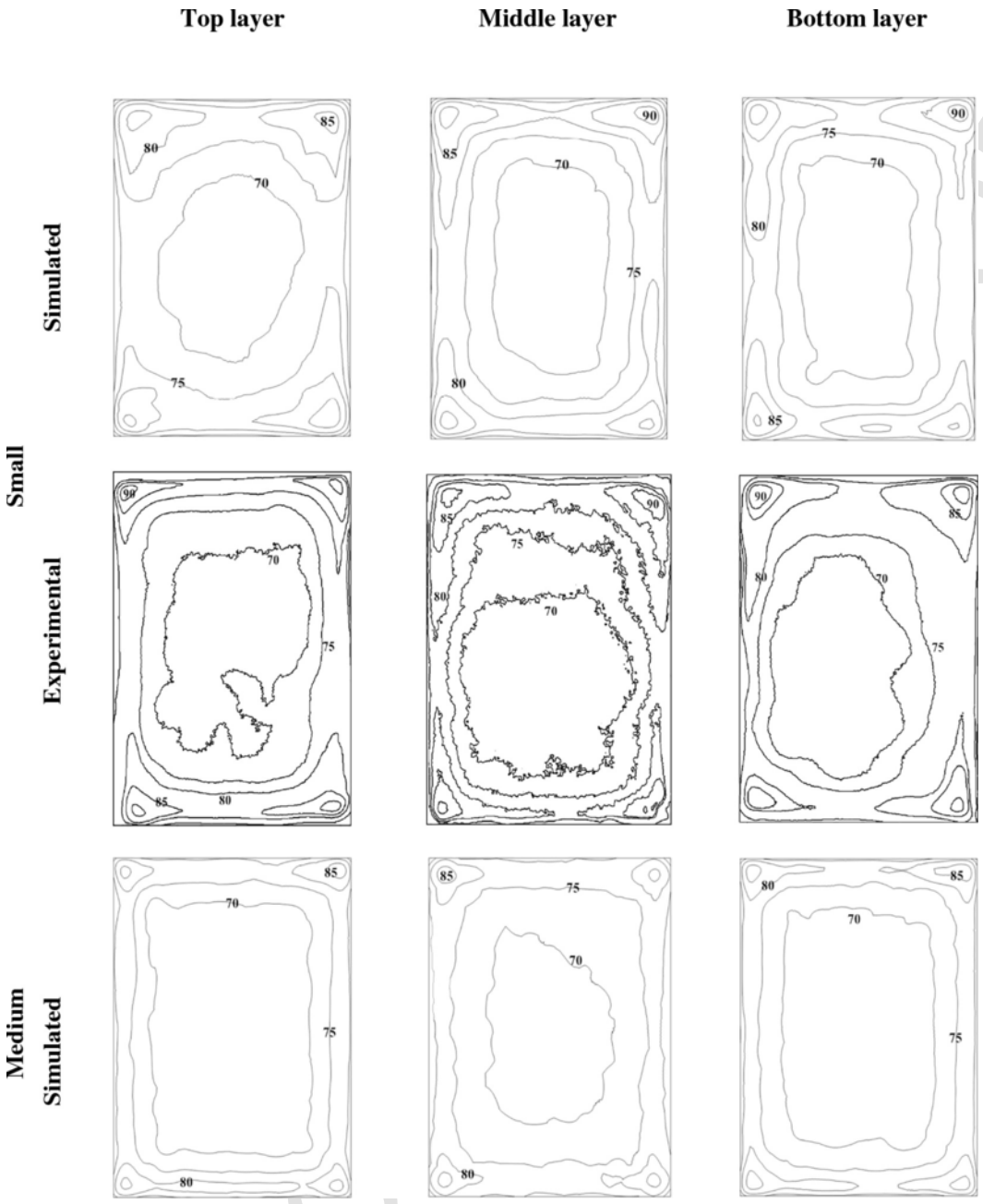

Fig. 6. Simulated and experimental temperature distributions (°C) of peanut kernels in top, middle and bottom layers placed in three dimensions of mica containers (large: 500 × 400 × 60 mm, medium: 400 × 300 × 60 mm, and small: 300 × 200 × 60 mm) without adding plates and blocks.

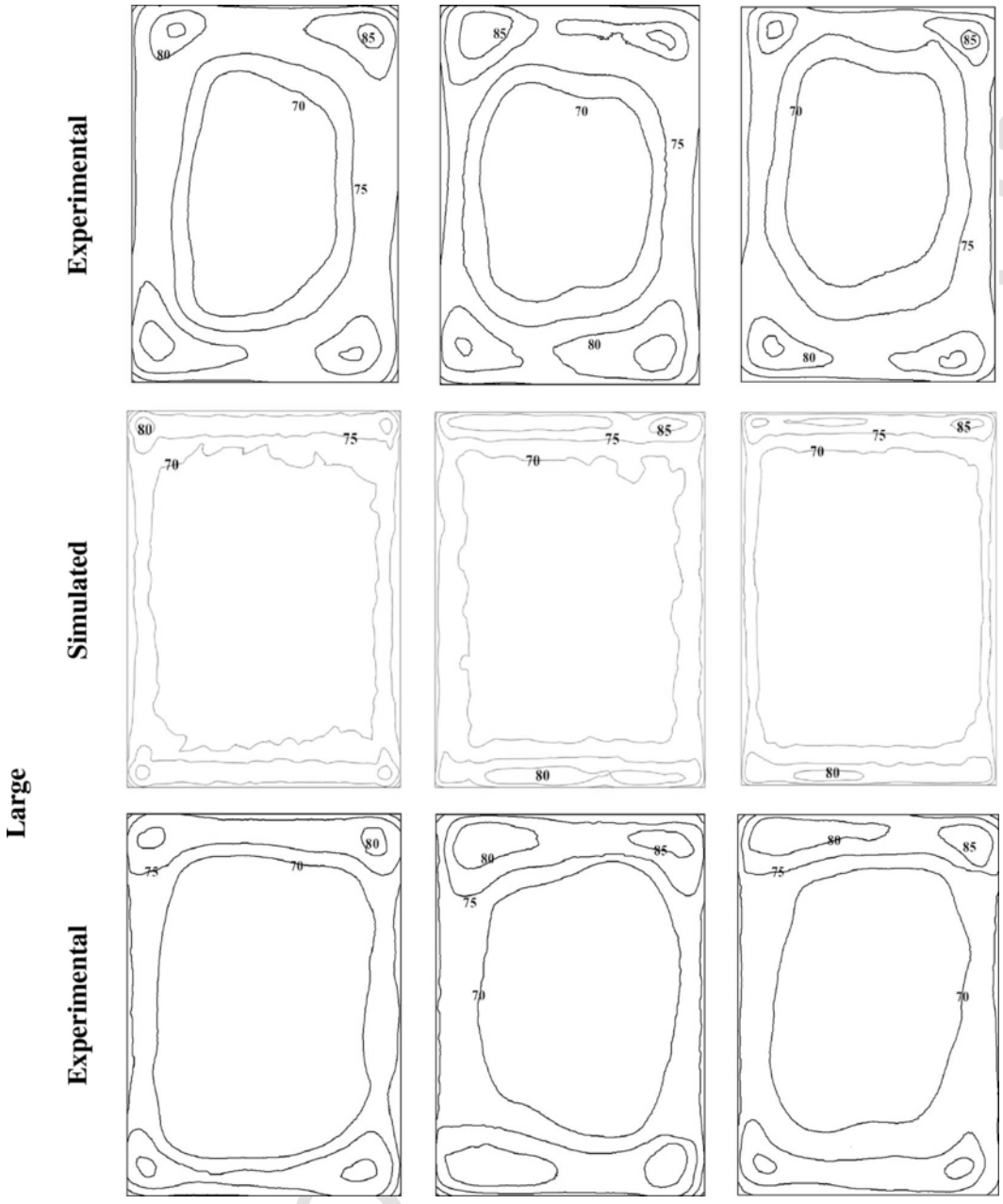

Fig. 6. (*Continued*)

Table 2
Simulated and experimental temperatures (Ave ± SD) in three different horizontal layers of peanuts in three different dimensions of mica containers without adding plates and blocks.

Container dimension (mm^3)	Layer	Simulated (°C)	Experimental (°C)
300 × 200 × 60	Top	75.78 ± 8.76	74.97 ± 6.99
	Middle	76.75 ± 8.56	75.3 ± 7.03
	Bottom	79.13 ± 8.53	78.59 ± 7.74
400 × 300 × 60	Top	75.79 ± 8.59	74.94 ± 6.97
	Middle	79.13 ± 8.94	78.49 ± 7.90
	Bottom	76.97 ± 9.06	76.48 ± 7.40
500 × 400 × 60	Top	74.67 ± 8.48	73.93 ± 6.85
	Middle	77.84 ± 8.23	76.63 ± 7.71
	Bottom	74.46 ± 8.86	75.04 ± 7.03

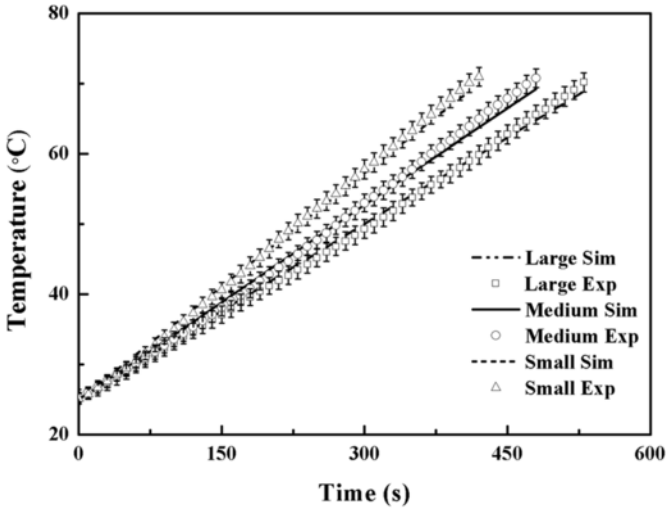

Fig. 7. Experimental and simulated central temperature-time histories of peanut samples at three different dimensions of mica containers when subjected to RF heating with electrode gap of 130 mm.

Table 3
Simulated volume average temperature (Avg) and uniformity index (UI) of peanuts when adding the mica plates with thickness of 5 mm on the small dimension container (300 × 200 × 60 mm) with length increased from 100 to 250 mm and width from 100 to 200 mm.

Length (mm)	Parameter	Width (mm)		
		100	150	200
100	Avg (°C)	78.61	78.66	79.07
	UI	0.180	0.176	0.179
150	Avg (°C)	78.75	79.01	79.42
	UI	0.175	0.173	0.174
200	Avg (°C)	78.74	79.28	80.14
	UI	0.167	0.168	0.174
250	Avg (°C)	79.05	79.65	80.73
	UI	0.168	0.170	0.178

Table 4
Simulated volume average temperature (Avg) and uniformity index (UI) of peanuts when adding the mica plates with thickness of 5 mm on the medium dimension container (400 × 300 × 60 mm) with length increased from 100 to 350 mm and width from 100 to 300 mm.

Length (mm)	Parameter	Width (mm)		
		100	200	300
100	Avg (°C)	78.23	78.41	78.61
	UI	0.182	0.177	0.178
150	Avg (°C)	78.37	78.52	79.02
	UI	0.180	0.171	0.176
200	Avg (°C)	78.47	78.95	79.54
	UI	0.176	0.169	0.174
250	Avg (°C)	78.65	79.22	79.78
	UI	0.174	0.165	0.170
300	Avg (°C)	78.82	79.51	80.30
	UI	0.172	0.164	0.173
350	Avg (°C)	78.90	79.55	80.69
	UI	0.172	0.165	0.178

Table 5
Simulated volume average temperature (Avg) and uniformity index (UI) of peanuts when adding the mica plates with thickness of 5 mm on the large dimension container (500 × 400 × 60 mm) with length increased from 100 to 400 mm and width from 100 to 400 mm.

Length (mm)	Parameter	Width (mm)			
		100	200	300	400
100	Avg (°C)	76.13	76.14	76.24	76.30
	UI	0.146	0.143	0.142	0.143
200	Avg (°C)	76.23	76.60	76.73	77.03
	UI	0.142	0.139	0.135	0.140
300	Avg (°C)	76.36	76.86	77.17	77.51
	UI	0.140	0.134	0.130	0.136
400	Avg (°C)	76.51	77.15	77.49	78.12
	UI	0.140	0.136	0.135	0.141

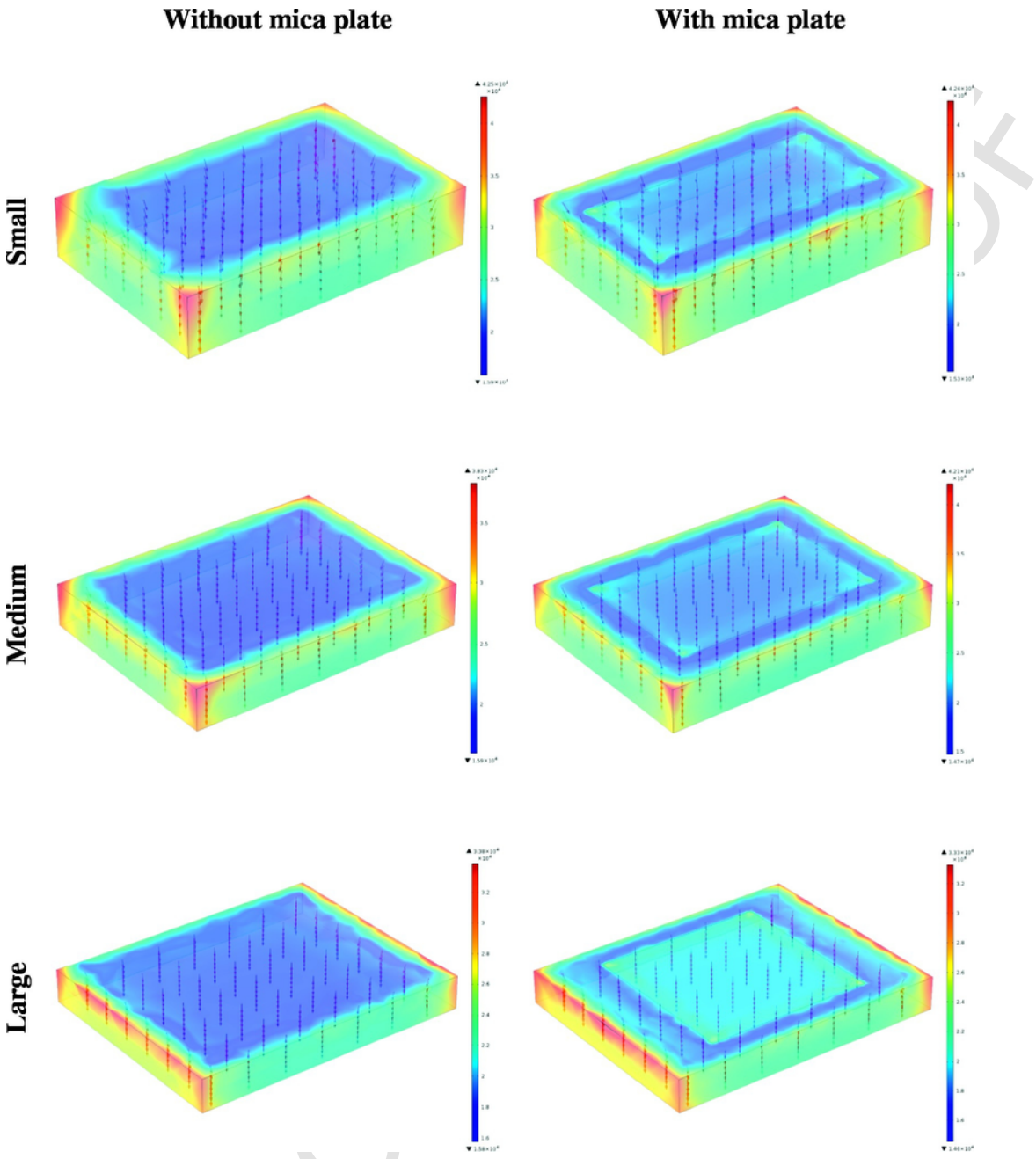

Fig. 8. Electric field intensity (V/m) and directions in peanut samples with and without adding mica plates with the size for the best heating uniformity in three dimensions of containers.

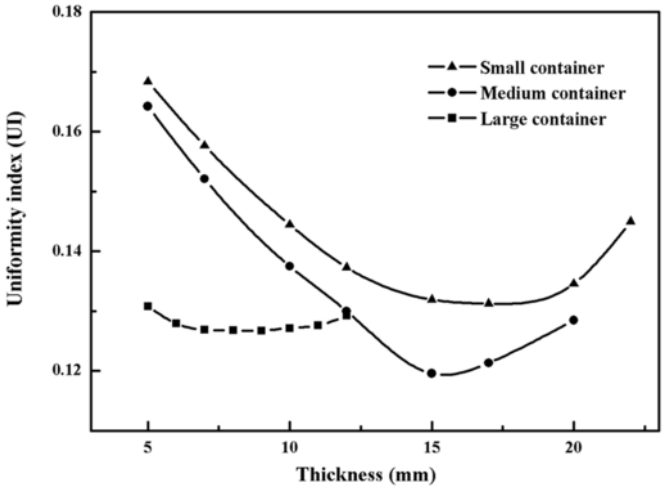

Fig. 9. Uniformity index (UI) of peanut samples with various thicknesses of mica plates with the size for the best heating uniformity in three containers.

Table 6
Simulated volume average temperature (Avg) and uniformity index (UI) of peanuts in the large container (500 × 400 × 60 mm) with various dimensions of polypropylene blocks after 530 s RF heating with a fixed electrode gap of 130 mm.

Width (mm)	Length (mm)	Depth (mm)					
		20		30		40	
		Avg (°C)	UI	Avg (°C)	UI	Avg (°C)	UI
150	250	77.57	0.139	78.30	0.137	79.08	0.136
	300	77.76	0.140	78.60	0.140	80.47	0.139
	350	77.82	0.142	78.89	0.140	79.67	0.142
250	250	78.23	0.138	79.48	0.136	80.65	0.135
	300	78.48	0.138	79.78	0.137	80.78	0.137
	350	78.55	0.140	80.00	0.140	81.17	0.139
350	250	78.88	0.139	80.47	0.136	82.05	0.134
	300	79.05	0.138	80.76	0.136	82.32	0.131
	350	79.13	0.140	81.00	0.137	82.76	0.133

References

Alfaifi, B., Tang, J., Jiao, Y., Wang, S.J., Rasco, B., Jiao, S.S., Sablani, S., 2014. Radio frequency disinfestation treatments for dried fruit: Model development and validation. Journal of Food Engineering 120, 268–276.

Birla, S.L., Wang, S., Tang, J., Hallman, G., 2004. Improving heating uniformity of fresh fruit in radio frequency treatments for pest control. Postharvest Biology and Technology 33 (2), 205–217.

Chen, L., Wang, K., Li, W., Wang, S., 2015. A strategy to simulate radio frequency heating under mixing conditions. Computers and Electronics in Agriculture 118, 100–110.

Chen, L., Huang, Z., Wang, K., Li, W., Wang, S., 2016. Simulation and validation of radio frequency heating with conveyor movement. Journal of Electromagnetic Waves & Applications 1–19.

Choi, C.T.M., Konrad, A., 1991. Finite element modeling of the RF heating process. IEEE Transactions on Magnetics 27 (5), 4227–4230.

COMSOL Material Library, 2012. COMSOL Multiphysics, V4.3a. Burlington, MA, USA.

Deshpande, S.D., Bal, S., 1999. Specific heat of soybean. Journal of Food Process Engineering 22 (6), 469–477.

Deshpande, S.D., Bal, S., Ojha, T.P., 2007. Bulk thermal conductivity and diffusivity of soybean. Journal of Food Processing & Preservation 20 (3), 177–189.

Farag, K.W., Marra, F., Lyng, J.G., Morgan, D.J., Cronin, D.A., 2010. Temperature changes and power consumption during radio frequency tempering of beef lean/fat formulations. Food and Bioprocess Technology 3 (5), 732–740.

Follett, P.A., Snook, K., Janson, A., Antonio, B., Haruki, A., Okamura, M., Bisel, J., 2013. Irradiation quarantine treatment for control of Sitophilus oryzae (Coleoptera: Curculionidae) in rice. Journal of Stored Products Research 52 (5), 63–67.

Fu, Y.C., 2008. Fundamentals and industrial applications of microwave and radio frequency in food processing. In: Food processing: Principles and applications. Blackwell, Iowa, USA, pp. 79–100.

Gao, M., Tang, J., Villa-Rojas, R., Wang, Y., Wang, S., 2011. Pasteurization process development for controlling salmonella in in-shell almonds using radio frequency energy. Journal of Food Engineering 104 (2), 299–306.

Hertwig, C., Kai, R., Ehlbeck, J., Knorr, D., Schlüter, O., 2015. Decontamination of whole black pepper using different cold atmospheric pressure plasma applications. Food Control 55, 221–229.

Hill, R.A., Blankenship, P.D., Cole, R.J., Sanders, T.H., 1983. Effects of soil moisture and temperature on preharvest invasion of peanuts by the aspergillus flavus group and subsequent aflatoxin development. Applied and Environmental Microbiology 45 (2), 628–633.

Hou, L., Huang, Z., Kou, X., Wang, S., 2016. Computer simulation model development and validation of radio frequency heating for bulk chestnuts based on single particle approach. Food and Bioproducts Processing 100, 372–381.

Huang, Z., Zhu, H.K., Wang, S., 2015. Finite element modeling and analysis of radio frequency heating rate in mung beans. Transactions of the ASABE 58 (1), 149–160.

Huang, Z., Zhu, H.K., Yan, R.J., Wang, S.J., 2015. Simulation and prediction of radio frequency heating in dry soybeans. Biosystems Engineering 129, 34–47.

Huang, Z., Marra, F., Wang, S.J., 2016. A novel strategy for improving radio frequency heating uniformity of dry food products using computational modeling. Innovative Food Science & Emerging Technologies 34, 100–111.

Huang, Z., Zhang, B., Marra, F., Wang, S., 2016. Computational modelling of the impact of polystyrene containers on radio frequency heating uniformity improvement for dried soybeans. Innovative Food Science & Emerging Technologies 33, 365–380.

Jeong, S.G., Kang, D.H., 2014. Influence of moisture content on inactivation of Escherichia coli O157:H7 and salmonella enterica serovar typhimurium in powdered red and black pepper spices by radio-frequency heating. International Journal of Food Microbiology 176 (1640), 15–22.

Jiao, S., Johnson, J.A., Tang, J., Mattinson, D.S., Fellman, J.K., Davenport, T.L., Wang, S., 2013. Tolerance of codling moth, and apple quality associated with low pressure/low temperature treatments. Postharvest Biology and Technology 85 (11), 136–140.

Jiao, Y., Tang, J., Wang, S.J., 2014. A new strategy to improve heating uniformity of low moisture foods in radio frequency treatment for pathogen control. Journal of Food Engineering 141, 128–138.

Jiao, Y., Shi, H.J., Tang, J.M., Li, F., Wang, S.J., 2015. Improvement of radio frequency (RF) heating uniformity on low moisture foods with polyetherimide (PEI) blocks. Food Research International 74, 106–114.

Jiao, S., Zhong, Y., Deng, Y., 2016. Hot air-assisted radio frequency heating effects on wheat and corn seeds: Quality change and fungi inhibition. Journal of Stored Products Research 69, 265–271.

Kanapitsas, A., Batrinou, A., Aravantinos, A., Markaki, P., 2015. Effect of γ-radiation on the production of aflatoxin B 1 by Aspergillus parasiticus in raisins (Vitis vinifera L.). Radiation Physics and Chemistry 106 (3), 327–332.

Marra, F., Lyng, J., Romano, V., Mckenna, B., 2007. Radio-frequency heating of foodstuff: Solution and validation of a mathematical model. Journal of Food Engineering 79 (3), 998–1006.

Mehdizadeh, M., 2009. Microwave/RF applicators and probes for material heating, sensing, and plasma generation a design guide. William Andrew; Elsevier Science distributor, Norwich, N.Y. Oxford.

Metaxas, A.C., 1996. Foundations of electroheat. A unified approach. Fuel and Energy Abstracts 37 (3), 193.

Romano, V., Marra, F., 2008. A numerical analysis of radio frequency heating of regular shaped foodstuff. Journal of Food Engineering 84 (3), 449–457.

Ryynänen, S., 1995. The electromagnetic properties of food materials: A review of the basic principles. Journal of Food Engineering 26 (4), 409–429.

Suhem, K., Matan, N., Nisoa, M., Matan, N., 2013. Inhibition of Aspergillus flavus on agar media and brown rice cereal bars using cold atmospheric plasma treatment. International Journal of Food Microbiology 161 (2), 107–111.

Tiwari, G., Wang, S., Tang, J., Birla, S.L., 2011. Analysis of radio frequency (RF) power distribution in dry food materials. Journal of Food Engineering 104 (4), 548–556.

Tiwari, G., Wang, S., Tang, J., Birla, S.L., 2011. Computer simulation model development and validation for radio frequency (RF) heating of dry food materials. Journal of Food Engineering 105 (1), 48–55.

Von Hippel, A.R., 1954. Dielectric properties and waves. Wiley, New York.

Wang, S., Ikediala, J.N., Tang, J., Hansen, J.D., Mitcham, E., Mao, R., Swanson, B., 2001. Radio frequency treatments to control codling moth in in-shell walnuts. Postharvest Biology and Technology 22 (1), 29–38.

Wang, S., Yue, J., Tang, J., Chen, B., 2005. Mathematical modelling of heating uniformity for in-shell walnuts subjected to radio frequency treatments with intermittent stirrings. Postharvest Biology and Technology 35 (1), 97–107.

Wang, S., Tang, J., Johnson, J.A., Cavalieri, R.P., 2013. Heating uniformity and differential heating of insects in almonds associated with radio frequency energy. Journal of Stored Products Research 55, 15–20.

Zhang, S., Zhou, L., Ling, B., Wang, S., 2016. Dielectric properties of peanut kernels associated with microwave and radio frequency drying. Biosystems Engineering 145, 108–117.

Zheng, A., Zhang, B., Zhou, L., Wang, S., 2016. Application of radio frequency pasteurization to corn (Zea mays L.): Heating uniformity improvement and quality stability evaluation. Journal of Stored Products Research 68, 63–72.

Zhou, L.Y., Wang, S.J., 2016. Industrial-scale radio frequency treatments to control Sitophilus oryzae in rough, brown, and milled rice. Journal of Stored Products Research 68, 9–18.

Zhou, L., Ling, B., Zheng, A., Zhang, B., Wang, S., 2015. Developing radio frequency technology for postharvest insect control in milled rice. Journal of Stored Products Research 62, 22–31.

Zhu, H., Huang, Z., Wang, S., 2014. Experimental and simulated top electrode voltage in free-running oscillator radio frequency systems. Journal of Electromagnetic Waves & Applications 28 (5), 606–617.